Silicon nanowire Biosensors for detection of cardiac troponin I (cTnI) with High sensitivity

Kihyun Kim, Chanoh Park, Donghoon Kwon, Donghoon Kim, M. Meyyappan, Sangmin Jeon, Jeong-Soo Lee

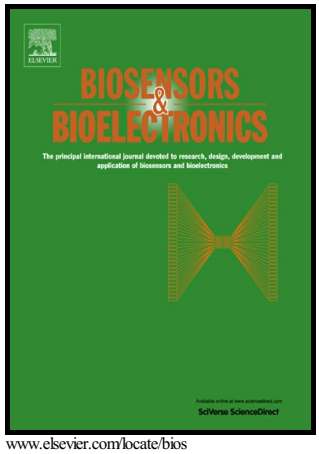

www.elsevier.com/locate/bios

PII: S0956-5663(15)30473-5
DOI: http://dx.doi.org/10.1016/j.bios.2015.10.008
Reference: BIOS8044

To appear in: *Biosensors and Bioelectronic*

Received date: 20 July 2015
Revised date: 30 September 2015
Accepted date: 2 October 2015

Cite this article as: Kihyun Kim, Chanoh Park, Donghoon Kwon, Donghoo Kim, M. Meyyappan, Sangmin Jeon and Jeong-Soo Lee, Silicon nanowir Biosensors for detection of cardiac troponin I (cTnI) with High sensitivity *Biosensors and Bioelectronic,* http://dx.doi.org/10.1016/j.bios.2015.10.008

Silicon Nanowire Biosensors for Detection of Cardiac Troponin I (cTnI) with High Sensitivity

Kihyun Kim[a], Chanoh Park[b], Donghoon Kwon[c], Donghoon Kim[d], M. Meyyappan [e], Sangmin Jeon[c], and Jeong-Soo Lee[b, d, *]

[a] Department of Creative IT Engineering and Future IT Innovation Lab., Pohang University of Science and Technology (POSTECH), Pohang 37673, Korea
[b] Division of IT-Convergence Engineering, Pohang University of Science and Technology (POSTECH), Pohang 37673, Korea
[c] Department of Chemical Engineering, Pohang University of Science and Technology (POSTECH), Pohang 37673, Korea
[d] Department of Electrical Engineering, Pohang University of Science and Technology (POSTECH), Pohang 37673, Korea
[e] NASA Ames Research Center, Moffett Field, California 94035, USA

ABSTRACT

We have demonstrated highly sensitive, label-free detection of cardiac troponin I (cTnI), a biomarker for diagnosis of acute myocardial infarction, using silicon nanowire field-effect transistors. A honeycomb-like structure is utilized for nanowire configuration to offer improved electrical performance and increased sensing area. The fabricated devices show n-type behavior with a relatively high ON-OFF current ratio, small sub-threshold swing and low gate leakage current. Monoclonal antibodies for cTnI were covalently immobilized on the nanowire surface, and the attachment of antibodies is clearly visualized by atomic force microscopy. The sensitivity with various concentrations of buffer solution was also investigated in order to determine the optimal buffer condition. The devices exhibit highest sensitivity under buffer solutions with low ion concentration. In addition, the limit of detection of the sensor is as low as ~5 pg/mL, the lowest reported in the literature to date and nearly an order of magnitude smaller than the suggested threshold limit. The fabricated devices demonstrate a good selectivity for detecting cTnI.

KEYWORDS: Honeycomb nanowire, Field-effect transistor, Biosensor, Cardiac troponin I, Limit of detection, Debye length

* Corresponding author.

E-mail address: ljs6951@postech.ac.kr (J.-S. Lee)

1. Introduction

Cardiovascular diseases have been the leading cause of death worldwide and the mortality from cardiovascular diseases is expected to increase rapidly due to the growth in aging population (Reiter et al., 2011; Kim and Cho, 2013). Acute myocardial infraction (AMI) or heart attack is the most common type of cardiovascular disease. The AMI occurs when a part of the heart muscle is damaged due to lack of blood supply, possibly caused by blockage of a coronary artery. The necrosis of heart muscle is irreversible and 85% of heart damage progresses within the first two hours after the onset of a heart attack, and delayed medical treatment increases the probability of mortality. Therefore, early and accurate diagnosis of AMI and prompt treatment are critical to increase the survival rate. The diagnosis of AMI has been traditionally done by monitoring the elevated concentration of biomarkers related to myocardial necrosis. Cardiac troponin I (cTnI), which is released only in response to cardiomyocyte necrosis, is used as one of the preferred biomarkers due to high specificity and high sensitivity (McDonnell et al., 2009). The National Academy of Clinical Biochemistry recommended that the 99th percentile of troponin concentrations from a healthy reference population is used as a cutoff (sometimes called a threshold) value for diagnosis of AMI. The diagnostic cutoff has decreased in the past decades, reaching recently to 40 pg/mL (Melanson et al., 2008).

The enzyme-linked immunosorbent assay (ELISA) has been widely used in clinical diagnostics for detecting cTnI because it ensures high diagnostic accuracy. However, the long diagnostic times, requirement of well-trained operator and expensive laboratory equipment are serious drawbacks of this approach. Several alternative techniques such as surface plasmon resonance (SPR) (Hu et al., 2006), electrochemiluminescence based biosensor (Shen et al.,

2011), fluorescence based biosensor (Nandhikonda and Heagy, 2011), and radioimmunoassay (RIA) (Apple et al., 1997), have been reported to overcome the drawbacks of ELISA. These methods require labeling which leads to increased detection time and complexity of the sensor device. For the early and accurate diagnosis of AMI, therefore, novel diagnostic tools with rapid detection time as well as high sensitivity need to be developed.

Silicon nanowire field-effect-transistors (Si-NW FETs) have recently received much attention as a powerful diagnostic platform because of the possibility for ultrasensitive, selective, real-time and label-free detection (Zheng et al., 2005; Gao et al., 2011). These advantages arise from their operation principle which is based on the gating effect of the antigen-antibody binding events on the NW surface. In addition, Si-NW FETs provide several advantages such as easy integration with signal processing circuit, low cost, and low device-to-device variation because these devices can be fabricated using commercial microfabrication technology. Thus, Si-NW FETs can be considered as one of the promising candidates for portable point-of-care devices. Since the first Si-NW pH sensor was demonstrated by Cui et al. (2001), the approach has been used for the detection of proteins, DNA and viruses.

The detection limit of cTnI for top-down fabricated FETs has recently been reported at near a hundred pg/mL, which is not sufficient for AMI diagnosis (Kong et al., 2012; Huang et al., 2013). The sensitivity and limits of detection (LOD) are largely dependent on the ionic concentration of the electrolyte, the amount of biomolecules bound to the nanowire surface, and the intrinsic electrical performance of the device itself. Novel FET structures with better intrinsic characteristics including sub-threshold swing (SS) have been proposed to improve these metrics (Ahn et al., 2010; Rigante et al., 2011; Sarkar et al., 2012; Buitrago et al., 2014) because better electrical characteristics can produce larger signal changes even with a small amount of surface

charges induced by the target biomolecules. However, the proposed structures in the literature require additional fabrication procedures and higher power consumption. In addition, long and suspended nanowires (which are typically only ~ 10 nm in diameter) between source/drain contacts pose mechanical stability problems. Arranging the nanowires in a honeycomb-like structure, in contrast, is mechanically more robust and provides superior intrinsic electrical performance and larger surface area than conventional straight-line nanowires (SLNW) with no additional fabrication steps and similar voltage operation (Rim et al., 2013, 2014; Kim et al., 2014). The superior intrinsic characteristics of the HCNW come from two reasons caused by the periodically repeating Y junctions. First, the HCNW has larger effective channel width than the SLNW. The change in drain current for a given change in gate voltage, $\Delta I_D/\Delta V_G$, is proportional to the aspect ratio W/L of the FETs and thus, the output signal change of the HCNW is improved compared to that of the SLNW. Second, the honeycomb structure can provide many optimized paths, which consist of unit nanowires with high conductivity, for the current flow between the source and drain compared with the SLNW. The honeycomb structure can achieve the improved sensing performance due to excellent electrical characteristics and increased surface area, which can raise the chance of binding events between the biomolecules and antibodies on the sensor surface. However, the devices with the honeycomb nanowire configuration have not been tested for their sensing characteristics before. Here, for the first time, we have used such a structure for biosensing application and demonstrated label-free, highly sensitive and selective detection of cTnI. Antibodies were successfully immobilized on the nanowire surface and confirmed using atomic force microscopy (AFM). The specific binding ability of the sensor was then ascertained through the detection of C-reactive protein (CRP) and alpha-fetoprotein (AFP). The influence of

Debye length on sensor response was also investigated for optimization of the sensing performance.

2. Materials and methods

2.1 Materials

Phosphate buffered saline (PBS. pH 7.4), 0.1M KCl, (3-aminopropyl)triethoxysilane (APTES, 99%), glutaraldehyde (50%), and bovine serum albumin (BSA) were purchased from Sigma-Aldrich (St. Louis, MO, USA). Absolute ethanol was purchased from Merck (Darmstadt, Germany). cTnI protein and its monoclonal antibodies (mAbs) were purchased from HyTest Ltd (Finland). CRP and AFP as control antigen were purchased from HBI (Anyang, Korea).

2.2 Fabrication of nanowire FETs

Honeycomb nanowire (HCNW) structures with light doping concentrations were used for the sensing channel of the FETs in order to enhance the sensitivity (Nair and Alam, 2007). The process flow is presented in Fig. S1 under Supporting Information. The devices were fabricated on silicon-on-insulator (SOI) substrates with 100 nm top-Si layer (boron-doped, ~10 Ω·cm) and 200 nm buried oxide layer. First, the device bodies were formed using conventional photolithography and inductively-coupled plasma reactive ion etching (ICP-RIE). Before the ion implantation process, 20 nm SiO_2 film was deposited using plasma enhanced chemical vapor deposition (PECVD) for preventing the out-diffusion of implanted ions during post-annealing process. Then, arsenic ions with a dose of 5×10^{15} cm^{-2} were implanted into the device bodies except the channel region, followed by annealing at 1000 °C for 20 s. Honeycomb nanowires were formed on the channel region by employing electron-beam lithography and ICP-RIE. The high-energy ion bombardment on the etched surface during ICP-RIE can create plasma-induced defects, which can cause degradation of the sensor performance in terms of sensitivity and reliability (Stern et al., 2007a). Therefore, the nanowire surface damaged by the plasma was

removed by 4 nm thick thermally grown sacrificial oxide, followed by immersing in diluted HF solution. The 5 nm thick SiO_2 gate dielectric was thermally grown in a furnace. Then, Ag/Ti (200 nm/20 nm) layers were deposited and patterned using conventional lift-off process to form Ag/AgCl pseudo-reference electrode (pRE), which served as the top-gate electrode. During this process, the source/drain contact pads were also defined to provide low contact resistance. The passivation layer of a 2 μm thick SU-8 was coated on the top of devices (excluding honeycomb nanowire, pRE, and contact pads). The passivation layer can play a critical role in preventing the current flow between the contact pads and aqueous solution during measurement. Finally, the embedded Ag/AgCl pRE was fabricated using an electrochemical method. 0.1 M KCl was dropped on the Ag electrode and a bias of 1 V was applied on the Ag electrode. Under constant bias, the top of Ag was converted to AgCl by reaction between Ag and Cl^- ions. Some SLNW devices were also fabricated on the same chip for comparison. Fig. 1(a) and (b) show the optical images of the fabricated HCNW FETs chip with 32 devices and an on-chip Ag/AgCl pRE. Fig. 1(c) shows the scanning electron microscope (SEM, JEOL JSM-7410F, Japan) image of the honeycomb nanowire (50 nm wide and 10 μm long) formed between the source and the drain. HCNW and SLNW devices were placed apart by 300 μm to minimize the influence due to any possible non-uniformity of the fabrication process (Fig. S2(a)). The SLNW devices are composed of 20-parallel NWs 50 nm wide and 10 μm long, as seen in Fig. S2(b).

2.3 Immobilization of antibodies on nanowire surface

In order to detect cTnI, monoclonal antibodies (mAbs) of cTnI were immobilized on the oxide surface of the devices. First, the devices were rinsed with ethanol to clean the surface and dried using N_2. Then, the devices were immediately dipped in 1% APTES in pure ethanol for 1h and

rinsed with pure ethanol followed by N_2 blow to remove unbound APTES molecules. During this treatment, the amine-functionalized surface was established due to the interaction between the silane group of APTES molecules and hydroxyl group of the oxide surface. Next, the devices with amine-functionalized surface were immersed in a solution of 5% glutaraldehyde in deionized (DI) water for 30 min to introduce aldehyde-terminated surface. After rinsing with DI water, the mAbs were covalently bound to the nanowire surface by dropping 1 μL of 1× PBS solution including 10 μg/mL cTnI mAbs on aldehyde-terminated surface followed by 1h incubation at room temperature in humid condition. The residues of mAbs were washed out using 1× PBS. Finally, to prevent nonspecific binding of proteins, the active aldehyde groups were blocked using 0.1% BSA in 1× PBS for 2h. The devices were stored in 1× PBS at 5°C. Fig. S3 provides a schematic diagram of the chemical process for mAbs immobilization. The samples were imaged by AFM (Veeco Dimension 3100, USA) in tapping mode to visualize the oxide surface after immobilization of mAbs.

2.4 Electrical characterization and biosensing experiments

Electrical measurements were performed using a semiconductor parameter analyzer (Keithley 4200, USA) at room temperature. Three contact terminals (source, drain, and Ag/AgCl pRE) were connected to probe needles to control the terminal voltages and measure the drain current I_D. The source terminal was connected to the ground (V_S = 0 V) for all the measurements. The gate voltage V_G was applied to the devices using the liquid gate system. For the initial electrical characteristics, the devices without any treatment were characterized in 0.01× PBS solution. Label-free and selective electrical detection of cTnI was carried out by monitoring the change in I_D-V_G curve of the functionalized devices with different cTnI concentrations. The concentrations

of cTnI were adjusted by dissolving and diluting pure cTnI in PBS solution. For the non-specific binding test, high concentrations of CRP (2.3 μg/mL) and AFP (1.2 μg/mL) were also prepared. PBS with volume of 30 μL and same incubation time was used for biosensing experiments. In addition, to investigate the Debye screening effect, PBS solutions with different ion concentration (1× PBS, 0.1× PBS, and 0.01× PBS) were prepared by dilution of 1× PBS solution with DI water.

3. Results and discussion

3.1 Electrical Characteristics of HCNW FETs

Fig. 2(a) shows the transfer curve (log-scale I_D-V_G) and the output curve (Log-scale I_G-V_G) of the fabricated devices. The corresponding linear-scale I_D-V_G curve is shown in Fig. S4. The devices show typical n-type FET behavior where the drain current (I_D) increases with gate voltage (V_G). Excellent electrical characteristics have been achieved with a high ON-OFF current ratio of ~10^6, a gate leakage current of less than 10^{-11} A, negligible hysteresis, small SS of 90 mV/dec, low threshold voltage (V_{TH}) of 0.58V and drain induced barrier lowering (DIBL) of 10 mV/V (SLNW: SS of 100 mV/dec and V_{TH} of 0.63V). As mentioned earlier, the superior intrinsic characteristics come from the enlarged effective channel width and increased current paths relative to the SLNW due to periodically repeating Y-shaped intersections. The HCNW FETs here exhibit smaller SS than the SLNW case as shown in our previous work (Rim et al., 2013, 2014; Kim et al., 2014). Hysteresis caused by the defects between the nanowire and the gate oxide can threaten sensor reproducibility. The negligible hysteresis of the fabricated devices here indicates that the devices have low level of defect density, which is attributed to the additional sacrificial oxidation and dHF etching. This was also independently verified by a

controlled comparison of devices with and without sacrificial oxidation wherein the devices subjected to sacrificial oxidation process indeed showed smaller hysteresis. The gate leakage current is another important parameter for biosensing, which is strongly dependent on the oxide quality or current path between the contacts through the aqueous solution. The gate leakage current should be kept at a low magnitude ($<10^{-11}$ A) during device operation. Our results indicate that the SU-8 layer successfully prevents the leakage current flow between the Ag/AgCl pRE and the source/drain electrode and assures a reliable operation. Besides the transfer characteristics, the output characteristics are shown in Fig. 2(b) and in common with conventional n-MOSFETs, the I_D is dependent on both the V_G and the V_D.

3.2 AFM analysis of antibodies immobilized on gate dielectric surface

Before the immobilization of mAbs on the HCNW, the chemical process (mentioned in section 2.3) was treated on bare oxide samples in order to verify the immobilization of mAbs on the oxide surface. As a control experiment, another bare oxide sample without any treatment was immersed in 1× PBS containing 10 μg/mL cTnI mAbs for 1h at room temperature. Fig. 3(a) illustrates the 3D AFM height images of the bare oxide surface with the chemical process after exposure to a solution containing cTnI mAbs. Many peaks are visible and the peak height is in the range of 1.5-8 nm with an average value of 4 nm. In contrast, the surface roughness was 0.2 nm in the bare oxide surface without the chemical process (Fig. S5), and no peak was observed over the entire surface of the samples. This comparison confirms that mAbs are successfully immobilized after the surface treatment. In addition, the observed mean peak height of 4 nm indicates that most mAbs were not vertically attached on the surface because the reported

vertical height of mAb is about 10 nm in the absence of aggregation (Bermudez and Forciniti, 2004).

3.3 Electrical detection of cTnI

After immobilization of mAbs on the NW devices, five devices were used for characterizing the sensitivity and the LOD. Fig. 3(b) shows the I_D-V_G curves of a representative functionalized device for various cTnI concentrations. As the cTnI concentration increases from 5 pg/mL to 5 ng/mL, the I_D-V_G curve shifts to the right direction (in the positive V_G direction). Other electrical parameters such as SS and transconductance (g_m) remain at the same values during the shift of the transfer curve. When the cTnI is exposed to an electrolyte with pH 7.5, it carries a negative charge because the isoelectric point (pI) of cTnI is around 5.2 (Peronnet et al., 2007). The surface has more negative charge with increasing cTnI concentration. Thus, the shift in the I_D-V_G curve can be explained by the negative charges of the bound cTnI on the gate oxide.

The sensitivity is normally defined as the normalized current change after the binding event of the target antigen ($S = |\Delta I_D|/I_{D0}$), where I_{D0} is the reference current which is set as the I_D of the functionalized device before the attachment of biomolecules and $\Delta I_D = I_{D1}$-I_{D0}. I_{D1} is the I_D of the functionalized device after the binding event. To determine the sensitive operation regime of the devices, the sensitivity was extracted for different values of I_{D0}. Fig. 3(c) shows the sensitivity as a function of the cTnI concentration for various values of I_{D0}. The calculated sensitivity is at its maximum with I_{D0} of 1 nA and then decreases as the I_{D0} is increased. The sensitivity dramatically drops at I_{D0} = 1.8 μA because the device operates in the saturation regime. From the transfer curves of the FETs (Fig. 3(c)), two distinct regimes are clearly formed, that is, the sub-

threshold regime ($V_G<V_{TH}$) and linear regime ($V_G>V_{TH}$). The I_D is less dependent on the gate voltage in the linear regime compared with the sub-threshold regime. When the device is operated in the sub-threshold regime, the I_D increases exponentially with increasing V_G. This relationship between I_D and V_G can be expressed using the SS parameter, which is defined as the additional V_G required for creating one decade increase of I_D. From Fig. 3(c), it turns out that the overall sensitivity extracted in the sub-threshold regime is at least 7 times higher than that in the linear regime due to the exponential increase of I_D behavior in the sub-threshold regime; this is consistent with previous observations (Gao et al., 2009).

It is previously reported that while the sensitivity of SLNW in the sub-threshold regime is higher than that in the linear regime, the signal to noise ratio (SNR) of SLNW in the sub-threshold regime is lower than that in the linear regime (Rajan et al., 2011). When a device is operated at high gate voltage (i.e., linear regime), however, the electrical characteristics are degraded as the biasing time increases. As the gate-bias voltage increases from the subthreshold regime to linear regime, the SNR increases and the stress-induced degradation becomes severe, and vice versa (Rim et al., 2014). This degradation can cause false positive (negative) error of the sensor and is characterized by measuring the I_D drift or V_{TH} shift after applying a given V_G during a given biasing time. Therefore, we extract the sensitivity at I_{D0} = 60 nA by considering both the SNR and the stress effect on the device performances.

3.4 Influence of Debye screening on cTnI detection

The sensitivity and LOD of FET-based sensors are limited by the Debye length (λ_D), i.e. the thickness of an electrical double layer (EDL) near the gate dielectric/buffer interface in an

electrolyte solution. Beyond the Debye length, the charges of biomolecules are screened by the dissolved ions. For aqueous solutions, the λ_D is given by (Stern et al., 2007b)

$$\lambda_D = \sqrt{\frac{\varepsilon_r \varepsilon_0 kT}{2q^2 I}} \tag{1}$$

$$I = N_A\left(\frac{1}{2}\sum_i C_i z_i^2\right) \tag{2}$$

where ε_r is the relative permittivity of the electrolyte, ε_0 is the vacuum permittivity, k is Boltzmann's constant, T is the temperature, N_A is the Avogadro number, q is the elementary charge, C_i is the concentration of ion species i, z_i is the valence of ion species i, and I is the ionic strength of the buffer. In order to investigate the Debye screening effect on sensitivity, PBS solutions with different ion concentrations (1× PBS, 0.1× PBS, and 0.01× PBS; ionic strength 180, 18, and 1.8 mM respectively) were prepared by dilution of 1× PBS solution with DI water. The calculated Debye lengths for the three cases according to Eq. (1) and Eq. (2) are ~ 0.7, 2.3 and 7.3 nm respectively. Fig. 3(d) shows the effect of buffer concentration on the sensitivity of the sensors. The sensitivity is improved as the ion concentration of the buffer solution decreases because the PBS with lower ion concentration shows longer λ_D, as described by Eq. (1) and Eq. (2). For the 5 pg/mL cTnI, the sensitivity in 0.01× PBS is about 2.5 times higher than that in 0.1× PBS due to increased λ_D. In contrast, the devices show no detection of cTnI up to high concentration (1 ng/mL) in 1× PBS solution where most of the cTnI charges are effectively screened at the oxide surface because the measured height of immobilized mAbs from AFM image (1.5-8 nm) is higher than the calculated Debye length (~ 0.7 nm). The optimal buffer condition for detecting cTnI using these devices is 0.01× PBS solution. Thus, the concentration of the buffer solution plays a critical role in charge-based sensors. However, extremely low salt

concentrations may not retain the biological activity of proteins (Lawal et al., 2005; Joucla et al., 2013).

3.5 Sensitivity enhancement by honeycomb structure

Fig. 4 shows the sensitivity versus logarithm of cTnI concentration at I_{D0} = 60 nA and 0.01× PBS solution. The solid line indicates the calibration curve to show the linear-log behavior between the sensitivity and cTnI concentration (C_{cTnI} [pg/mL]). The calibration curve can be obtained from the log fit as $S = 0.1872 \times \log C_{cTnI} + 0.106$. The sensitivity of the HCNW biosensor is about 8 times higher than previously reported value in the literature for single Si-NW biosensor (Kong et al., 2012), as seen in Fig. S6. The sensitivity of the honeycomb structure is about 20 % higher than that for the SLNW devices (Fig. S6). Table 1 summarizes the LOD of cTnI biosensors from this work and previous reports in the literature. The present results represent the lowest LOD to date and this value is 8 times lower than the current diagnostic cutoff for acute myocardial infarction (40 pg/mL). The LOD of the fabricated sensor is well above 3 times the theoretical LOD which is defined using the 3-Sigma method. As mentioned before, the higher sensitivity and lower LOD of HCNW devices come from the geometrical advantage of honeycomb nanowires, which can provide smaller SS and larger surface area than the SLNW devices. The sensitivity of the FET-based sensor can be improved by decreasing the SS because smaller SS can produce larger ΔI_D with the same amount of surface charges induced by the biomolecules. The honeycomb nanowire can provide ~1.5 times larger surface area than the straight nanowire array for the same nanowire geometry, suggesting that the probability of binding events between cTnIs and mAbs can be improved and thus the number of cTnIs bound to the sensing surface can be enhanced.

3.6 Specificity test: control protein detection

Two control experiments were conducted in order to confirm the selective detection capability of the HCNW sensors and the results are shown in Fig. 5. The functionalized devices were tested with CRP and AFP, which are used as control biomarkers, to evaluate the effects of non-specific binding. Fig. 5(a) and Fig. 5(b) show non-specific binding effects of the CRP and AFP for the functionalized sensors, respectively. The I_D-V_G curve shows very little change after adding a high concentration of CRP (2.3 μg/mL) and AFP (1.23 μg/mL), indicating that there is no non-specific binding with cTnI mAbs. The non-specific binding of control biomarkers is restricted because the BSA molecules fill in the binding sites on the nanowire surface after the immobilization of mAbs. These results confirm a satisfactory level of specificity while detecting target biomarkers, even in a solution containing both non-target and target biomarkers.

4. Conclusion

We have presented results for the label-free detection of cardiac biomarker (cTnI) with exceptional sensitivity and high specificity. The nanowire biosensors consist of lightly doped honeycomb nanowires and embedded Ag/AgClpRE fabricated using a top-down approach. The detection limit obtained (~5 pg/mL) is the lowest reported to date and 8 times smaller than the recommended diagnostic cutoff of AMI. Excellent specificity was demonstrated through non-specific binding tests. The results here suggest that the present nanowire biosensor is very promising for clinical diagnosis of the AMI. Future work would continue to investigate this potential for the sensitive detection of other key cardiac biomarkers such as myoglobin and

cardiac reactive protein, multiplexing capability of a NW FET sensor array for the simultaneous detection of multiple markers and test results for clinical samples.

Acknowledgment

This work was in part supported by National Research Foundation (NRF) (No. 2013R1A1A2007094), by the MSIP (Ministry of Science, ICT and Future Planning), Korea, under the "ICT Consilience Creative Program" (IITP-2015-R0346-15-1007) supervised by the IITP (Institute for Information & communications Technology Promotion), and by the Agency for Defense Development (ADD-14-02-06-20), Korea.

Appendix A. Supplementary Information

Supplementary date associated with this article can be found in the online version at http://

References

Ahn, J.-H., Choi, S.-J., Han, J.-W., Park, T.J., Lee, S.Y., Choi, Y.-K., 2010. Nano Lett. 10, 2934-2938.

Apple, F.S., Falahati, A., Paulsen, P.R., Miller, E.A., Sharkey, S.W., 1997. Clin. Chem. 43, 2047-2051.

Bermudez, O., Forciniti, D., 2004. J. Chrom. B 807, 17-24.

Buitrago, E., Badia, M.F.-B., Georgiev, Y.M., Yu, R., Lotty, O., Holmes, J.D., Nightingaled, A.M., Guerina, H.M., Ionescua, A.M., 2014. Sens. Actuators B:Chem. 199, 291-300.

Cheng, Y., Chen, K.-S., Meyer, N.L., Yuan, J., Hirst, L.S., Chase, P.B., Xiong, P., 2011. Biosens. Bioelectron. 26, 4538-4544.

Cui, Y., Wei, Q., Park, H., Lieber, C.M., 2001. Science 293, 1289-1292.

Gao, A.R., Lu, N., Dai, P.F., Li, T., Pei, H., Gao, X.L., Gong, Y.B., Wang,Y.L., Fan, C.H., 2011. Nano Lett. 11, 3974-3978.

Gao, X.P.A., Zheng, G., Lieber, C.M., 2009. Nano Lett. 10, 547-552.

Guo, H.S., He, N.Y., Ge, S.X., Yang, D., Zhang, J.N., 2005a. Talanta 68, 61-66.

Guo, H.S., Zhang, J.N., Xiao, P.F., Nie, L.B., Yang, D., He, N.Y., 2005b. Jour. of Nanosci. Nanote. 5, 1240-1244.

Hu, W.P., Hsu, H.Y., Chiou, A., Tseng, K.Y., Lin, H.Y., Chang, G.L., Chen, S.J., 2006. Biosens. Bioelectron. 21, 1631-1637.

Huang, C.-W., Huang, Y.-J., Yen, P.-W., Tsai., H.-H., Liao, H.-H., Juang, Y.-Z., Lu, S.-S., Lin, C.-T., 2013. Lab on a Chip 13, 4451-4459.

Joucla, G., Le Sénéchal, C., Bégorre, M., Garbay, B., Santarelli, X., Cabanne, C., 2013. J. Chromatogr. B Analyt. Tehchnol. Biomed. Life Sci. 942–943, 126-133.

Kim, K., Rim, T., Park, C., Kim, D., Meyyappan, M., Lee, J.-S., 2014. Nanotechnology 25, 345501.

Kim, R.-H., Cho, G., 2013. Hum. Fac. Ergo.in Manuf. Ser. Indus. 23, 198-212.

Kim, W.-J., Kim, B.K., Kim, A., Huh, C., Ah, C.S., Kim, K.-H., Hong, J., Park, S.H., Song, S., Song, J., Sung, G.Y., 2010. Anal. Chem. 82, 9686-9693.

Kong, T., Su, R., Zhang, B., Zhang, Q., Cheng, G., 2012. Biosens. Bioelectron. 34, 267-272.

Lawal, O.S., Adebowale, K.O., Ogunsanwo, B.M., Sosanwo, O.A., Bankole, S.A., 2005. Food Chem. 92, 681-691.

Mahajan, V.S., Jarolim, P., 2011. Circulation 124, 2350-2354.

McDonnell, B., Hearty, S., Leonard, P., O'Kennedy, R., 2009. Clin. Biochem. 42, 549-561.

Nair, P.R., Alam, M.A., 2007. IEEE Trans. Electron Devices 54, 3400-3408.

Nandhikonda, P., Heagy, M.D., 2011. J. Am. Chem. Soc. 133, 14972-14974.

Periyakaruppan, A., Gandhiraman, R.P., Meyyappan, M., Koehne, J.E., 2013. Anal. Chem. 85, 3858-3863.

Peronnet, E., Becquart, L., Martinez, J., Charrier, J.P., Jolivet-Reynaud, C., 2007. Clin. Chim. Acta 377, 243-247.

Rajan, N.K. Routenberg, D.A., Reed, M. A., 2011. Appl. Phy. Lett. 98, 264107.

Reiter, M., Twerenbold, R., Reichlin, T., Haaf, P., Peter, F., Meissner, J., Hochholzer, W., Stelzig, C., Freese, M., Heinisch, C., Breidthardt, T., Freidank, H., Winkler, K., Campodarve, I., Gea, J., Mueller, C., 2011. Eur. Heart. J. 32, 1379-1389.

Rigante, S., Lattanzio, L., Ionescu, A. M., 2011. Microelec. Eng. 88, 1864-1866.

Rim, T., Kim, K., Kim, S., Baek, C.-K., Meyyappan, M., Jeong, Y.-H., Lee, J.-S., 2013. IEEE Electron Device Lett. 34, 1059-1061.

Rim, T., Meyyappan, M., Baek, C.-K., 2014. Nanotechnology 25, 505501.

Sarkar, D., Banerjee, K., 2012. Appl. Phys. Lett. 100, 143108.

Shen, W., Tian, D.Y., Cui, H., Yang, D., Bian, Z.P., 2011. Biosens. Bioelectron. 27, 18-24.

Stern, E., Klemic, J.F., Routenberg, D.A., Wyrembak, P.N., Turner-Evans, D.B., Hamilton, A.D., LaVan, D.A., Fahmy, T.M., Reed, M.A., 2007a. Nature 445,519-522.

Stern, E., Wagner, R., Sigworth, F.J., Breaker, R., Fahmy, T.M., Reed, M.A., 2007b. Nano Lett. 7, 3405-3409.

Zhang, B., Morales, A.W., Peterson, R., Tang, L., Ye, J.Y., 2014. Biosens. Bioelectron. 58, 107-113.

Zheng, G., Patolsky, F., Cui, Y., Wang, W.U., Lieber, C.M., 2005. Nat. Biotechnol. 23, 1294–1301.

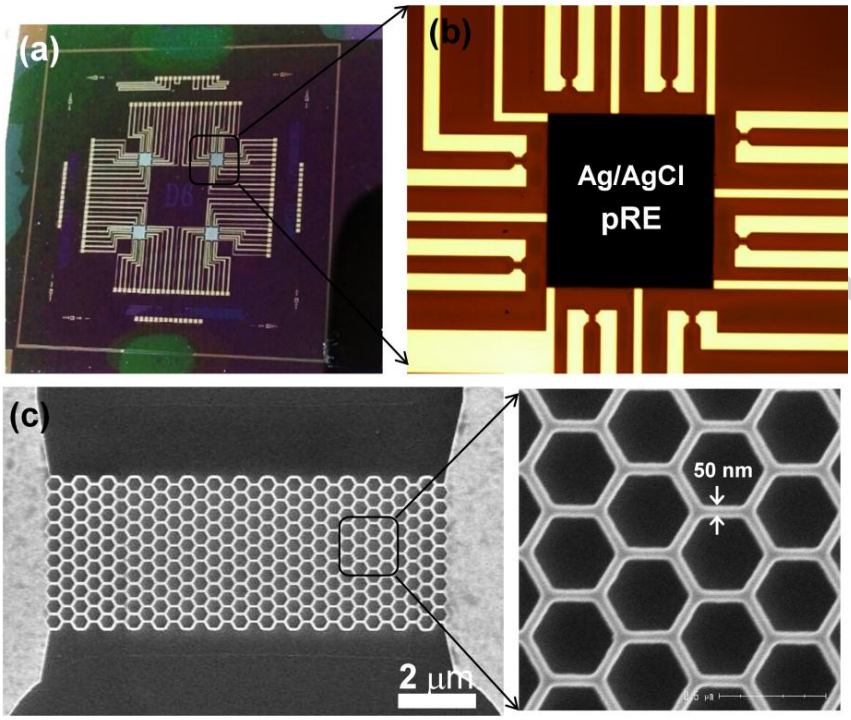

Fig. 1. (a) and (b) Optical images of the fabricated HCNW FETs. (c) SEM image of a honeycomb nanowire.

×

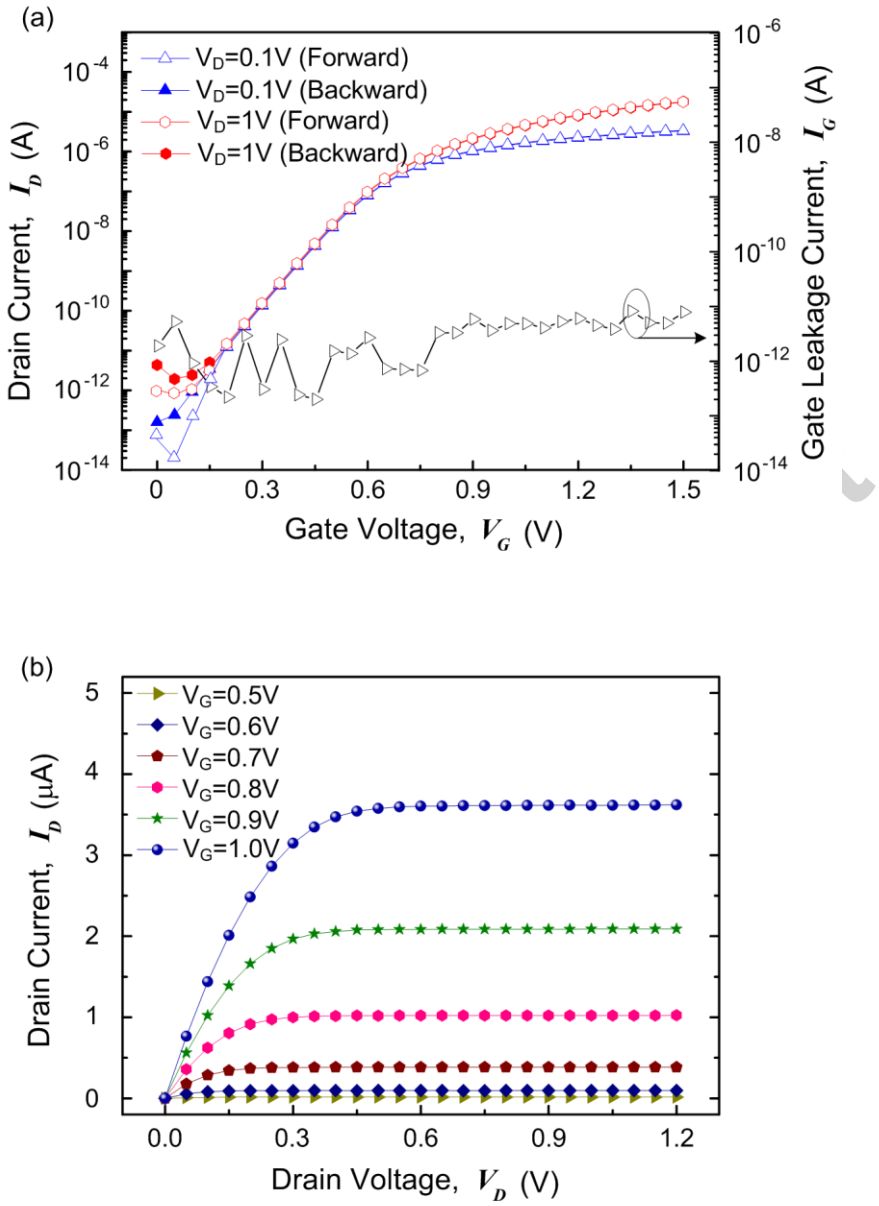

Fig. 2. Electrical characteristics of the fabricated HCNW devices. (a) Log-scale I_D–V_G curve (left axis) and Log-scale I_G–V_G curve (right axis) and (b) The I_D–V_D characteristics.

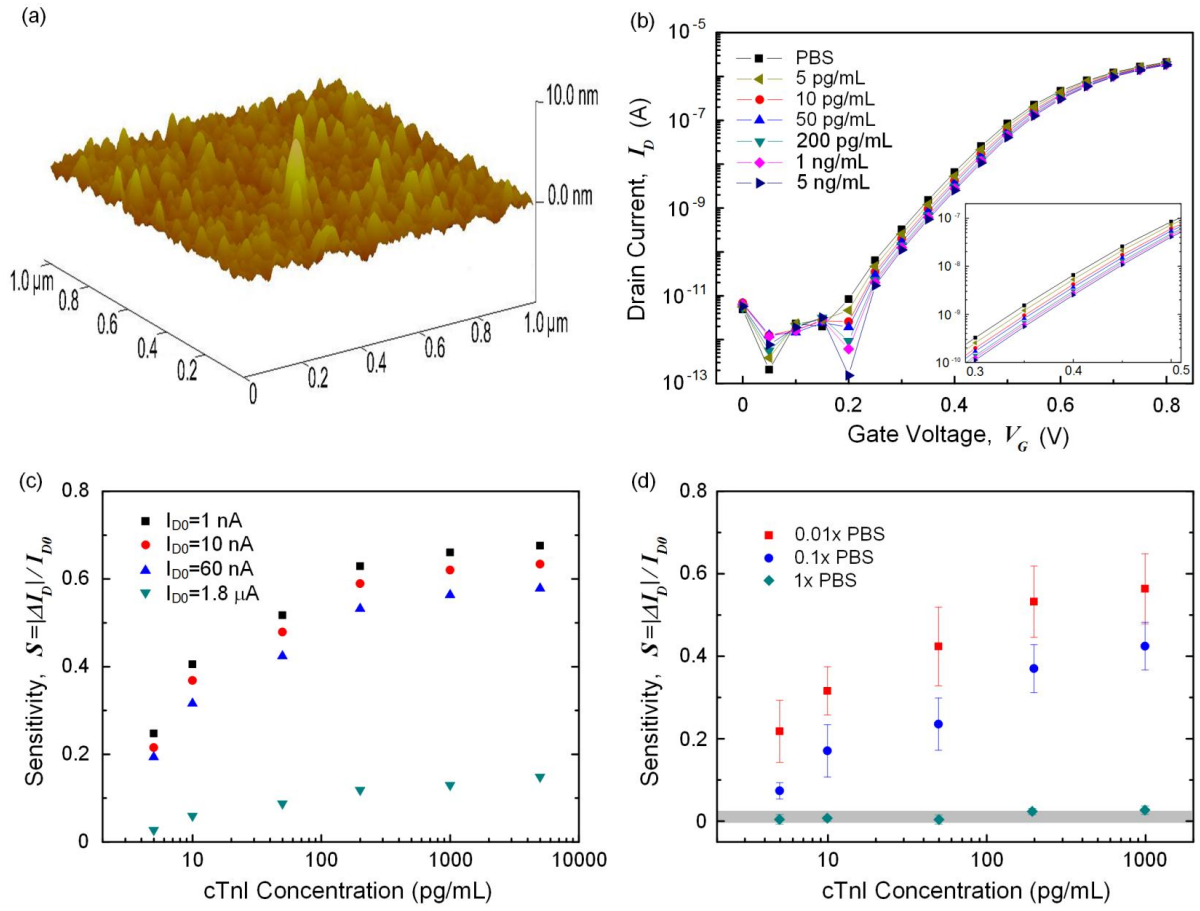

Fig. 3. (a) 3D AFM height images of the oxide surface with chemical treatment after exposure to a solution of cTnI antibodies. (b) Measured I_D-V_G characteristics (Log-scale) of a functionalized HCNW sensor for various cTnI concentrations. (c) Average sensitivity vs. logarithm of cTnI concentration for various values of I_{D0}. (d) Sensitivity vs. log of cTnI concentration in various phosphate buffer solutions: 0.01 ×PBS, 0.1× PBS, and 1× PBS.

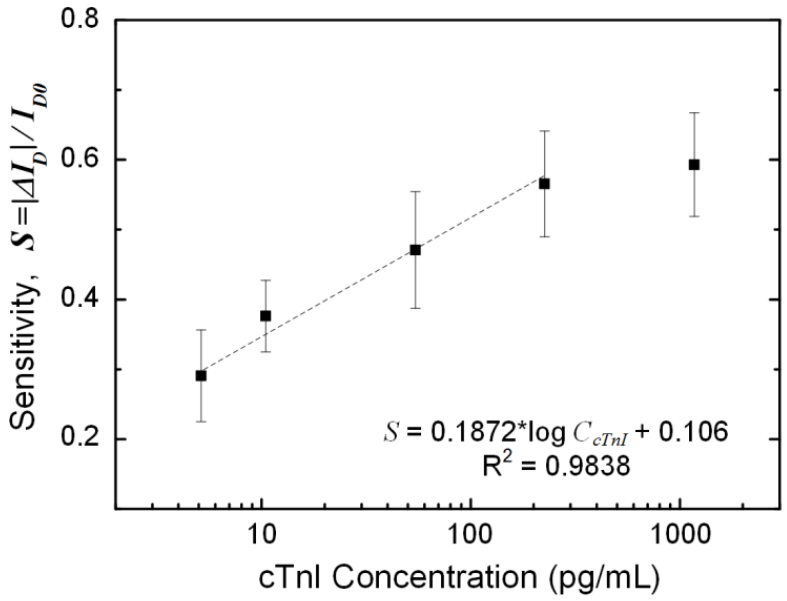

Fig. 4. Sensitivity vs. logarithm of cTnI concentration at I_{D0} = 60 nA and 0.01 ×PBS. Dotted lines represent the log fit: S = 0.1872*log C_{cTnI} +0.106.

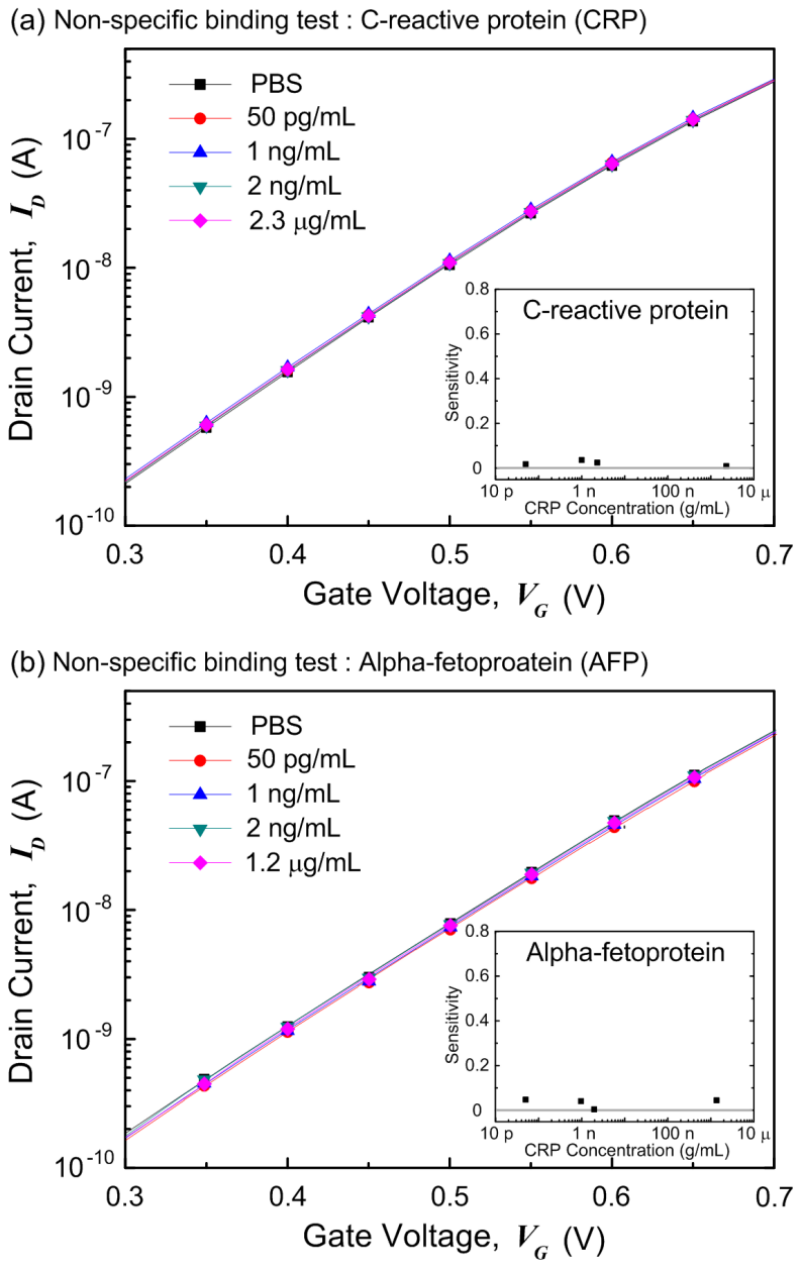

Fig. 5. Control experiments: (a) Non-specific binding test with CRP with the functionalized HCNW BioFETs. Inset: Sensitivity vs. CRP concentration. (b) Non-specific binding test with AFP with the functionalized HCNW BioFETs. Inset: Sensitivity vs. AFP concentration.

Table 1. Comparison of the limit of detection for cTnI biosensors.

Types	Materials	Limit of detection (ng/mL)	Ref.
FET	SnO_2 nanowire	2	Cheng et al. (2011)
Electrochemical immunoassay	MCM-41 mesoporous	0.5	Guo et al. (2005a)
Electrochemical immunoassay	Silver enhancement	0.8	Guo et al. (2005b)
Photonic crystal biosensor	Silica and silicon	0.1	Zhang et al. (2014)
FET	Silicon nanowire	0.092	Kong et al. (2012)
Guided-mode resonance (GMR)	GMR filter chips	0.05	Kim et al. (2010)
Nanoelectrode arrays	Carbon nanofiber	0.2	Periyakaruppan et al. (2013)
FET	Si nanowire	0.005	This work

Graphical abstract

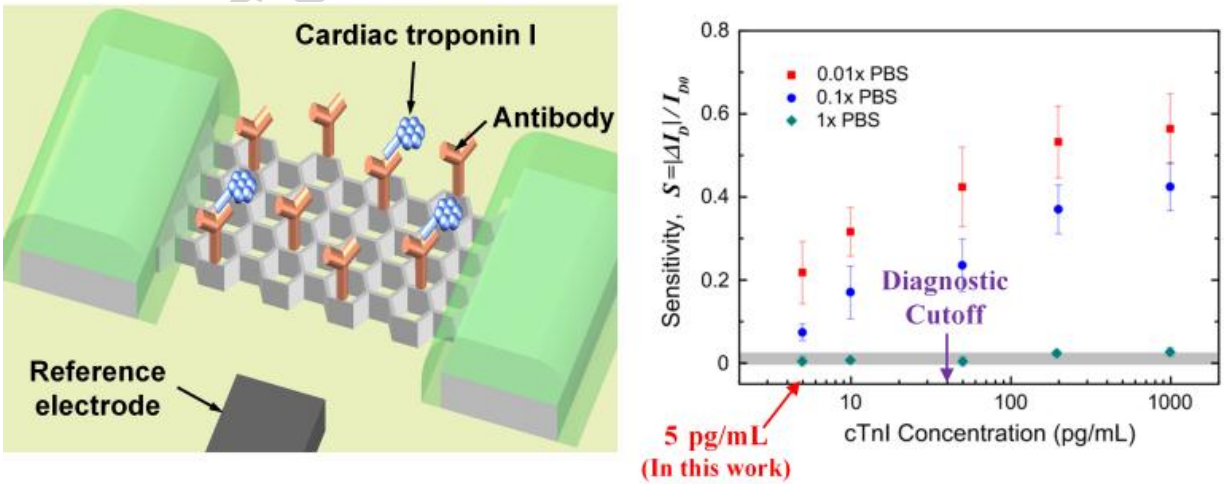

Highlights

► We fabricated novel silicon nanowire biosensors using honeycomb nanowire structure.

► The HCNW FETs show excellent electrical characteristics.

► The HCNW devices exhibit exceptional sensitivity and selectivity for detecting cTnI.

► Our devices show 8 times lower detection limit than the suggested cutoff at 5 pg/mL.

► Effect of Debye length was analyzed using AFM results and biosensing experiments.